Equivalence between condensation and boiling in a Lennard-Jones fluid

I. Sanchez-Burgos, P. Montero de Hijes, P. Rosales-Pelaez, C. Vega, and E. Sanz
Departamento de Química Física, Facultad de Ciencias Químicas, Universidad Complutense de Madrid, 28040 Madrid, Spain

(Received 7 August 2020; revised 1 November 2020; accepted 30 November 2020; published 28 December 2020)

Condensation and boiling are phase transitions highly relevant to industry, geology, and atmospheric science. These phase transitions are initiated by the nucleation of a drop in a supersaturated vapor and of a bubble in an overstretched liquid, respectively. The surface tension between both phases, liquid and vapor, is a key parameter in the development of such nucleation stage. Whereas the surface tension can be readily measured for a flat interface, there are technical and conceptual limitations to obtain it for the curved interface of the nucleus. On the technical side, it is quite difficult to observe a critical nucleus in experiments. From a conceptual point of view, the interfacial free energy depends on the choice of the dividing surface, being the surface of tension the one relevant for nucleation. We bypass the technical limitation by performing simulations of a Lennard-Jones fluid where we equilibrate critical nuclei (both drops and bubbles). Regarding the conceptual hurdle, we find the relevant cluster size by searching the radius that correctly predicts nucleation rates and nucleation free energy barriers when combined with Classical Nucleation Theory. With such definition of the cluster size we find the same value of the surface tension for drops and bubbles of a given radius. Thus, condensation and boiling can be viewed as two sides of the same coin. Finally, we combine the data coming from drops and bubbles to obtain, via two different routes, estimates of the Tolman length, a parameter that allows describing the curvature dependence of the surface tension in a theoretical framework.

DOI: 10.1103/PhysRevE.102.062609

I. INTRODUCTION

Understanding first-order phase transitions is of great importance to many fields, ranging from biology [1] to atmospheric science [2], physics [3], geology [4], and industry [5,6].

In the absence of impurities or external surfaces, first-order phase transitions start with the emergence of a nucleus of the stable phase in the bulk of the parent metastable phase [7,8]. A nucleus is "critical" if it is big enough so that it has a 50% chance to either grow or redissolve.

Although the emerging phase is more stable, the presence of an unfavourable interface between the nucleus and the parent phase can delay to a great extent the phase transition. Thus, for instance, alkane vapors can be saturated thousands of times over their vapor pressure before condensation takes place [9], alkane liquids can be substantially superheated above the boiling temperature [10–12], or liquid water can be supercooled up to ∼60 K below melting until it freezes [13–16].

Therefore, the surface tension, γ, or the free energy per unit area between both phases, plays a key role in the development of first-order phase transitions. Whereas γ can be readily measured for a flat interface at equilibrium—at least between fluid phases [17]—it cannot be directly probed for curved interfaces, which is the relevant case for nucleation. Moreover, the fact that critical nuclei are nanoscopic objects makes it very difficult to observe them in experiments, let alone measure their γ. The usual strategy is to infer γ by combining a theoretical description of nucleation with measurements of the nucleation rate (the number of nuclei that appear per unit of time and volume) [7,17–19]. This approach relies on the validity of theoretical approximations that are difficult to assess.

Computer simulations do have access to the time and length scales relevant for the observation of critical nuclei. However, whereas the methodology and theoretical framework for computing γ for flat interfaces is very well established [20–29], that for curved interfaces is still under development [30–32]. One of the key issues is that γ for curved interfaces depends on the location of the interface, which can be defined in different ways [32,33]. The current situation is that the dependence of γ with the curvature of the interface is contradictory between different groups [18,30–32,34–44]

In this work we address fundamental questions regarding the liquid-vapor interface with computer simulations. It has been shown in different simulation works that spherical nuclei can be equilibrated at constant volume and temperature in finite systems [35,44–53]. Recently, we showed with simulations of bubbles [54] and crystals [55] that nuclei thus equilibrated are critical, in agreement with Density Functional Theory (DFT) predictions [56,57]. On the other hand, we have extensively developed recently the so-called Seeding method [58–61] to study nucleation phenomena. This method consists in obtaining with simulations the properties of critical clusters and "plugging" them in the Classical Nucleation Theory (CNT) formalism [62–65] to obtain predictions of the nucleation rate and of the γ-curvature dependence. This approach has been successful for a wide range of

systems [54,58,59,61,66–70], and we use it here to study condensation. In particular, we apply Seeding at constant volume both to condensation and to cavitation for a Lennard-Jones model.

Since Seeding relies on CNT, it is necessary to validate it by comparing its predictions with rigorous calculations that do not rely on such a framework. We do so by computing nucleation rates via Umbrella Sampling (US) [71,72] and direct brute force simulations [73] as well as by testing the consistency of the γ-curvature dependence obtained via Seeding with the value for a flat interface.

All consistency tests are successfully passed for our Seeding simulations provided that the nucleus surface is identified with that where the density is the average between the density of both phases ("equidensity" surface). Therefore, we identify the equidensity surface with the surface of tension. On the other hand, we directly compare the condensation of liquid drops in a supersaturated vapor with the cavitation of vapor bubbles in an overstretched liquid. We find that, for a given temperature, drops and bubbles of the same radius have the same γ when using the equidensity definition of the surface of tension. Finally, we estimate the Tolman length [74], a parameter useful to predict the γ-curvature dependence, via two different routes, as recently proposed in Ref. [55].

II. SIMULATION DETAILS

The Lennard-Jones model potential, as well as the simulation details, are the same as in our previous work [54,70]. In particular, we study the truncated and force-shifted Lennard-Jones (TSF-LJ) potential [75], a model for which the vapor-liquid transition has been previously investigated [70,75–77]:

$$U_{\text{TSF-LJ}}(r) = U_{\text{LJ}}(r) - U_{\text{LJ}}(r_c) - (r - r_c)U'_{\text{LJ}}(r_c), \quad (1)$$

where $U_{\text{LJ}}(r)$ is the standard 12-6 Lennard-Jones potential and $U'_{\text{LJ}}(r)$ is its first derivative. The interaction potential is truncated and shifted at $r_c = 2.5\sigma$, where σ is the particle's diameter and ϵ the depth of the untruncated Lennard-Jones potential. Unless otherwise specified, all magnitudes in this work are given in Lennard-Jones reduced units [54]. Thus, the reported temperatures are reduced by ϵ/k_B, distances by σ, densities by σ^{-3}, pressures by ϵ/σ^3, times by $\tau = \sqrt{m\sigma^2/\epsilon}$ (where m is the particle mass), interfacial free energies by ϵ/σ^2, and nucleation rates by $1/(\tau\sigma^3)$.

We use cubic boxes with periodic boundary condition and the molecular dynamics (MD) LAMMPS package [78] to perform all simulations of this work. The equations of motion are integrated with a leap-frog algorithm [79].

In the MD Seeding simulations we used a time step of 0.0012. The system was kept at constant temperature using the Nosé-Hover thermostat [80] with a relaxation time of 0.46.

For the MD simulations used within the US scheme we set the time step for the integration of the motion equations to 0.0012. The relaxation times for the Nóse-Hover thermostat and barostat were 0.46 and 1.6, respectively.

All simulations are carried out at $T = 0.785$. The coexistence pressure at such a temperature for the model is $p_{\text{coex}} = 0.0267$. We determined this value, refined with respect to that of 0.026 previously published [75], by running long ($4 \times 10^5\,\tau$) MD *NVT* (i.e in the canonical ensemble) simulations with an elongated box ($50 \times 17 \times 17$) where the vapor and the liquid were put in contact at the temperature of interest. The average pressure normal to the interface in such a simulation corresponds to p_{coex}.

III. SEEDING OF CONDENSATION

This work is based on a recent publication where we demonstrate how to compute bubble nucleation rates in an overstretched Lennard-Jones fluid by equilibrating critical bubbles in the *NVT* ensemble, an approach we call "*NVT*-Seeding" [54]. The Seeding method, originally developed to study crystal nucleation [58–61], and more recently applied to vapor cavitation [54,70,81], consists in combining CNT [62–65] with computer simulations to estimate nucleation free energy barrier heights, ΔG_c, interfacial free energies, γ, and, most importantly, nucleation rates, J.

According to CNT, the Gibbs free energy barrier for the nucleation of a spherical liquid drop is given by the following expression:

$$\Delta G = \gamma A - V\Delta p, \quad (2)$$

where V and A are the volume and the area of the drop, respectively. By maximizing Eq. (2) assuming a spherical drop shape one obtains both the height of the nucleation free energy barrier,

$$\Delta G_c = \frac{2\pi R_c^3 \Delta p}{3}, \quad (3)$$

where R_c is the critical droplet radius and Δp is the pressure difference between the interior of the drop and the surrounding vapor, and the number of particles in the critical drop,

$$N_c = (32\pi\rho_l\gamma^3)/(3\Delta p^3), \quad (4)$$

where ρ_l is the critical drop number density and γ is the liquid-vapor surface tension. By substituting in the equation above N_c by the droplet volume $(4/3\pi R_c^3)$ times ρ_l one recovers the Laplace equation:

$$\Delta p = \frac{2\gamma}{R_c}. \quad (5)$$

This derivation shows that the Laplace equation, which is valid when the droplet surface is located at the the surface of tension, is implicit in CNT. Consequently, R_c should be identified with the radius of tension, R_s. This is an important point that we will use later in the paper.

The CNT prediction for the nucleation rate of drops is given by [7]

$$J = A_0\rho_{\text{vap}}\exp\left(-\frac{\Delta G_c}{k_B T}\right), \quad (6)$$

where k_B is the Boltzmann constant, ρ_{vap} is the density of the vapor phase that multiplied by $\exp(-\frac{\Delta G_c}{k_B T})$ gives the number density of critical clusters, and A_0 is a kinetic prefactor.

A_0 is computed as the product of the Zeldovich factor, Z, and the rate of attachment to the critical nucleus, f^+ [7,63]:

$$A_0 = Zf^+. \quad (7)$$

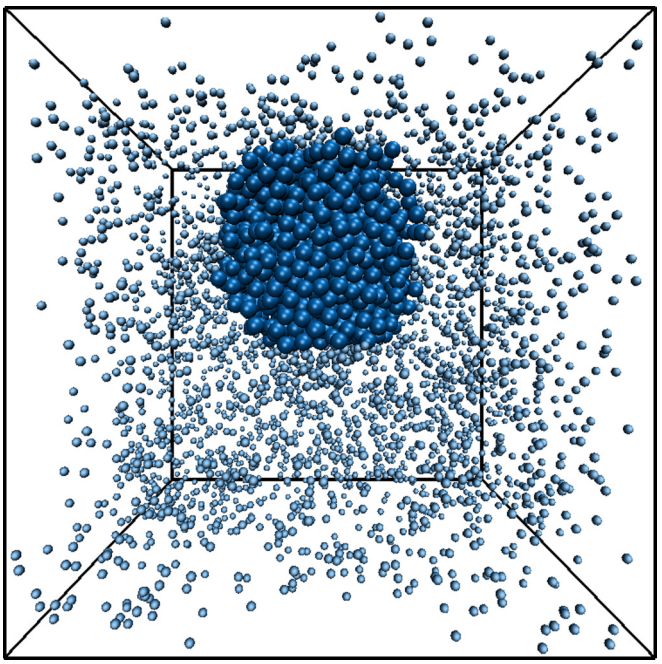

FIG. 1. Snapshot of a critical drop equilibrated in the *NVT* ensemble at $T = 0.785$ surrounded by supersaturated vapor. The droplet radius is about 6.8, and the density of the surrounding vapor 0.0550.

Z takes into account the establishment of a steady state, and, according to CNT, is given by [7,62,63]

$$Z = \sqrt{\frac{|\Delta G(N)''|_{N_c}}{2\pi k_B T}} = \sqrt{\frac{\Delta p}{6\pi k_B T \rho_l N_c}} = \sqrt{\frac{\Delta p}{8\pi^2 k_B T \rho_l^2 R_c^3}}, \tag{8}$$

where N_c is the number of particles in the drop and $|\Delta G_c(N)''|_{N_c}$ is the curvature of $\Delta G(N)$ evaluated at the barrier top.

The attachment rate, f^+, can be estimated by multiplying the collision frequency of the vapor per unit of wall area given by the kinetic theory of gases (ktg) by the area of the critical bubble:

$$f^+_{\rm ktg} = \sqrt{\frac{k_B T}{2\pi m}} \left(\frac{6\sqrt{\pi} N_c}{\rho_l} \right)^{2/3}, \tag{9}$$

where the subscript "ktg" stresses the fact that this expression of the attachment rate is based on the kinetic theory of gases. Combining this equation with Eqs. (8), (4), and (5), the following kinetic prefactor is obtained:

$$A_0^{\rm ktg} = \sqrt{\frac{\Delta p R_c}{\pi m}} \frac{\rho_{\rm vap}}{\rho_l}. \tag{10}$$

The equations above are quite powerful, because only R_c, Δp, and the density of both phases are required to obtain key nucleation parameters such as free energy barriers, interfacial free energies, and ınucleation rates. The Seeding method consists in performing simulations of a cluster of the stable phase surrounded by the mestastable phase (a liquid drop surrounded by supersaturated vapor in our case as shown in Fig. 1) to compute R_c, Δp, ρ_l, and $\rho_{\rm vap}$ in order to get "cheap" estimates of ΔG_c, γ, and, most importantly, J through the expressions above.

The main drawback of Seeding is that the definition of R_c is not unique. Therefore, the resulting free energy barrier depends on the specific definition of R_c. This contrasts with rigorous simulation methods like US [73,82] or with theoretical approaches like DFT [83–85] where the nucleation free energy does not depend on the criterion chosen to measure the nucleus size, which can be estimated *a posteriori* via, e.g., the nucleation theorem [86–88] (although in the particular case of DFT an approximate functional needs to be proposed so that the results do also contain approximations). To assess the suitability of our choice to compute R_c we complement Seeding with US simulations.

A. R_c, Δp, ρ_l, and $\rho_{\rm vap}$

We use the NVT ensemble to run the simulations of the drops given that in such an ensemble critical nuclei are naturally equilibrated and stabilized for long times [54,55]. We equilibrate drops in 10 different systems. The edge of the cubic simulation box, L, and the total number of particles in each system, N_T, are reported in Table I. A large number of particles are used to minimize finite-size effects [52,54,89]. Each system was simulated for about 10^3 Lennard-Jones times of equilibration and 2×10^5 of production.

To prepare the initial configuration we cut a spherical liquid drop from a bulk liquid simulation and insert it in a bulk vapor box removing the overlapping vapor particles. The liquid drop is cut with a certain tentative radius, but the precise number of particles in each phase is not crucial given that equilibrium is reached along the course of the NVT simulation.

From a simulation of a drop surrounded by supersaturated vapor one can obtain an average radial density profile starting from the center of the drop as that shown in Fig. 2 (to find the drop center in each configuration we use a strategy similar to that described in our previous work [54] consisting in this case in identifying the maxima of density profiles computed along each cartesian coordinate). Following Refs. [54,70], we obtain R_c from such a density profile as the distance at which the density is average between the liquid and the vapor plateaux. This is indicated with a vertical dashed line in Fig. 2. We refer to this way of obtaining R_c as the "equidensity" criterion. The R_c's thus obtained in our *NVT*-Seeding simulations are also reported in Table I. Other definitions of R_c are in principle as valid as the equidensity criterion [70,84,85]. We argue later in the paper that our R_c definition is a good one because it makes Seeding predictions consistent with independent calculations of γ, J, or ΔG_c.

To get $\Delta p = p_l - p_{\rm vap}$ we obtain first the vapor density, $\rho_{\rm vap}$, by counting the number of particles outside a sphere concentric with the drop but with a larger radius (we use a sphere radius 7σ larger than that of the drop, but we have checked for a few selected cases that any value beyond $\sim 5\sigma$ gives the same result). $\rho_{\rm vap}$ is given by the number of particles outside the sphere divided by the L^3 minus the sphere volume. We then use the bulk vapor equation of state to infer $p_{\rm vap}$ from $\rho_{\rm vap}$. We report $p_{\rm vap}$ and $\rho_{\rm vap}$ in Table I. We have checked for all studied systems that $p_{\rm vap}$ coincides with the overall virial

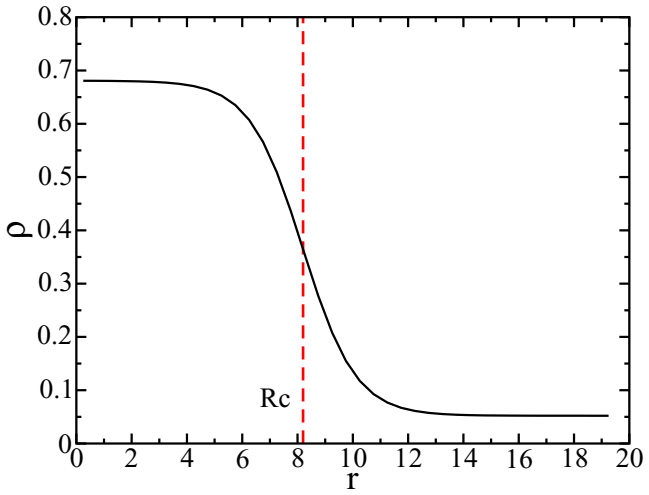

FIG. 2. Density profile of a critical drop equilibrated in the *NVT* ensemble at $T = 0.785$ surrounded by supersaturated vapor. The droplet radius, indicated by a red vertical line, is given by the point at which $\rho(r)$ takes an average value between both plateaux (equidensity criterion). The density profile corresponds to the system labeled as IV in Table I.

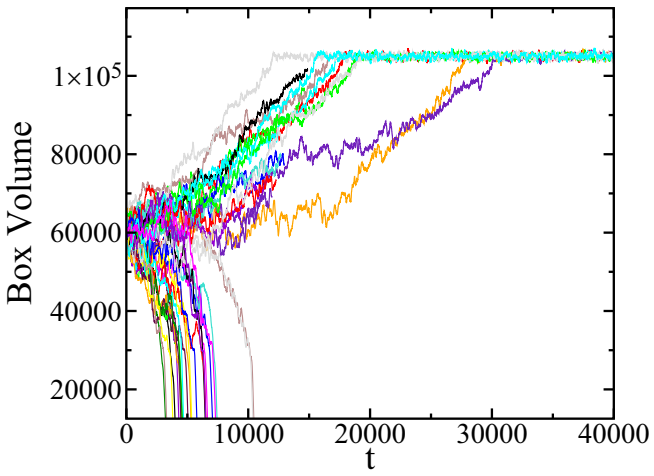

FIG. 3. Box volume vs time in *NpT* simulations starting from 40 configurations taken from the *NVT*-Seeding simulation labeled IX in Table I. The imposed pressure is the average viral pressure of the *NVT*-Seeding run.

pressure of the system. On the other hand, p_l is obtained, as in our previous work [54,70], by assuming equal chemical potential between the critical drop and the surrounding vapor:

$$\int_{p_{\rm coex}}^{p_{\rm vap}} \frac{1}{\rho_{\rm vap}(p)}\, dp = \int_{p_{\rm coex}}^{p_l} \frac{1}{\rho_l(p)}\, dp, \tag{11}$$

where $p_{\rm coex}$ is the coexistence pressure and $\rho_{\rm vap}(p)$ and $\rho_l(p)$ are the bulk vapor and bulk liquid number densities at pressure p, respectively. In Table I we report p_l and Δp for all studied systems. Once p_l is known, ρ_l, also reported in the table, can be easily computed from the bulk liquid equation of state. In all cases, this computation of ρ_l, based on the equality of chemical potential between both phases, is consistent with that obtained from the density profiles. For instance, for system IV we get $\rho_l = 0.0680$, which is fully consistent with the first plateau observed in the density profile shown in Fig. 2. This means that the mechanical pressure and the thermodynamic pressure inside the drop coincide, a matter of current debate for solid-liquid nucleation [90].

There has been much simulation, theoretical, and experimental work devoted to study of the formation of nuclei confined at constant volume [32,44,48,91–99]. In Refs. [54,55] we showed with simulations that nuclei equilibrated in the *NVT* ensemble are critical because they have equal chances to grow or shrink when simulated in the *NpT* (i.e isothermal isobaric ensemble) at the same temperature and at the average pressure along the *NVT* run. Based on this result, we opted to study here drop nucleation in the *NVT* ensemble, where statistics is better because clusters remain stable for very long times [54]. Stabilizing nuclei to gain time to study their properties is something quite desirable. An alternative strategy to the use of constant volume simulations is to pin the nucleus to a heterogeneous solid substrate [100].

Despite having already shown the equivalence between stable (*NVT*) and critical (*NpT*) nuclei for cavitation [54], we check here for one of the *NVT*-Seeding simulations if the drops equilibrated at constant volume and temperature do correspond to a Gibbs free energy maximum. In Fig. 3 we show the evolution of the box volume in *NpT* simulations started from 40 independent configurations gathered along the *NVT*-Seeding trajectory labeled IX in Table I. The imposed pressure is the average virial pressure along the *NVT*-Seeding

TABLE I. *NVT*-Seeding data for the different drops studied in this work at $T = 0.785$.

Label	L	N_T	ρ_l	$\rho_{\rm vap}$	p_l	$p_{\rm vap}$	Δp	R_c	γ	$\Delta G_c/(k_BT)$	$A_0^{\rm ktg}$	$A_0^{\rm af}$	$\log_{10}(J)$
I	38.019	3774	0.6833	0.05690	0.09279	0.03161	0.0612	5.86	0.1792	32.8	0.028		−17.1
II	39.160	4291	0.6811	0.05496	0.0846	0.03092	0.0537	6.82	0.1831	45.5	0.028		−22.6
III	39.160	4373	0.6801	0.05414	0.08095	0.03063	0.0503	7.15	0.1800	49.2	0.027		−24.2
IV	39.160	4510	0.6797	0.05384	0.07961	0.03052	0.0491	7.48	0.1835	54.8	0.027	0.030	−26.6
V	39.160	4623	0.6792	0.05342	0.07769	0.03037	0.0473	7.79	0.1843	59.7	0.027		−28.8
VI	39.160	4796	0.6782	0.05277	0.07468	0.03013	0.0446	8.20	0.1827	65.5	0.027	0.036	−31.3
VII	39.160	4964	0.6783	0.05269	0.07432	0.03010	0.0442	8.49	0.1878	72.3	0.027		−34.2
VIII	39.160	5163	0.6776	0.05216	0.07181	0.02991	0.0419	8.86	0.1856	77.8	0.027		−36.6
IX	39.160	5435	0.6771	0.05176	0.06989	0.02976	0.0401	9.30	0.1865	86.0	0.026		−40.2
X	85.264	34519	0.6761	0.05105	0.06638	0.02949	0.0369	9.99	0.1843	98.2	0.026		−45.5

run. Roughly, in 50% of the cases the box expands (the drop dissolves), and in the other half of the cases the box shrinks (the drop grows). This result supports the use of *NVT* to study drop condensation in the same manner that we used for bubble cavitation and crystal nucleation [54,55]. Furthermore, the equivalence between clusters equilibrated at constant volume and critical nuclei has been recently proven with DFT theoretical arguments for crystallization (see supplementary material of Ref. [57]).

Having computed R_c, Δp, ρ_{vap}, and ρ_l we have everything needed to obtain γ, ΔG_c and J according to the equations presented in Sec. III. We report the values for these variables in Table I and plot them in Figs. 4(a)–4(c) versus the vapor pressure with black dots. In the following section we comment on each of these graphs.

B. γ, ΔG_c, and J

1. γ

As shown in Fig. 4(a) the prediction we obtain from Seeding is that γ decreases as the vapor supersaturation increases. This trend is in agreement with previous work [35,47]. Accordingly, using the capillarity approximation (i.e., that γ is pressure independent) would be erroneous. The green square in Fig. 4(a) corresponds to the surface tension at coexistence [70] obtained through the pressure tensor [101] in an *NVT* simulation of a liquid and a vapor at contact. The trend of the Seeding data is fully consistent with the coexistence value, as shown by the linear fit in the figure. This is a good consistency test, although the γ values provided by Seeding could still be incorrect despite the fact that they extrapolate correctly to coexistence. Therefore, a test for Seeding predictions away from coexistence is needed.

2. ΔG_c

To further test our Seeding results we compare ΔG_c obtained with Seeding with that computed via US. In Fig. 4(b), where we plot ΔG_c versus the vapor pressure, black solid dots correspond to Seeding and red ones to US (details on US calculations are described in Sec. IV). Whereas Seeding predictions rely on the validity of CNT and on a proper definition of R_c, US calculations are rigorous and independent on the criterion to identify the nucleus size [73]. On the other hand Seeding is much "cheaper" than US from a computational point of view. As a matter of fact, Seeding has access to much higher nucleation barriers than US. The accordance between Seeding and US shown in Fig. 4 is excellent, which gives us great confidence in Seeding predictions. The choice of the equidensity surface to identify the drop radius has proven correct. If we use another criterion, such as the Gibbs (equimolar) dividing surface, the agreement between Seeding and US deteriorates [empty black symbols in Fig. 4(b)]. To compute R_e, the radius associated with the Gibbs dividing surface, we use $N_T = N_l + N_{\text{vap}}$ where $N_l = 4/3\pi R_e^3 \rho_l$ and $N_{\text{vap}} = [V_T - (4/3\pi R_e^3)]\rho_{\text{vap}}$, where V_T is the volume of the simulation box and the densities ρ_l and ρ_{vap} are obtained as described in Sec. III A.

In a recent publication on cavitation (nucleation of bubbles instead of drops) we compared the performance of different criteria to identify the cluster radius and found that the equidensity criterion also made Seeding predictions consistent with other rigorous calculations [70]. Therefore, identifying

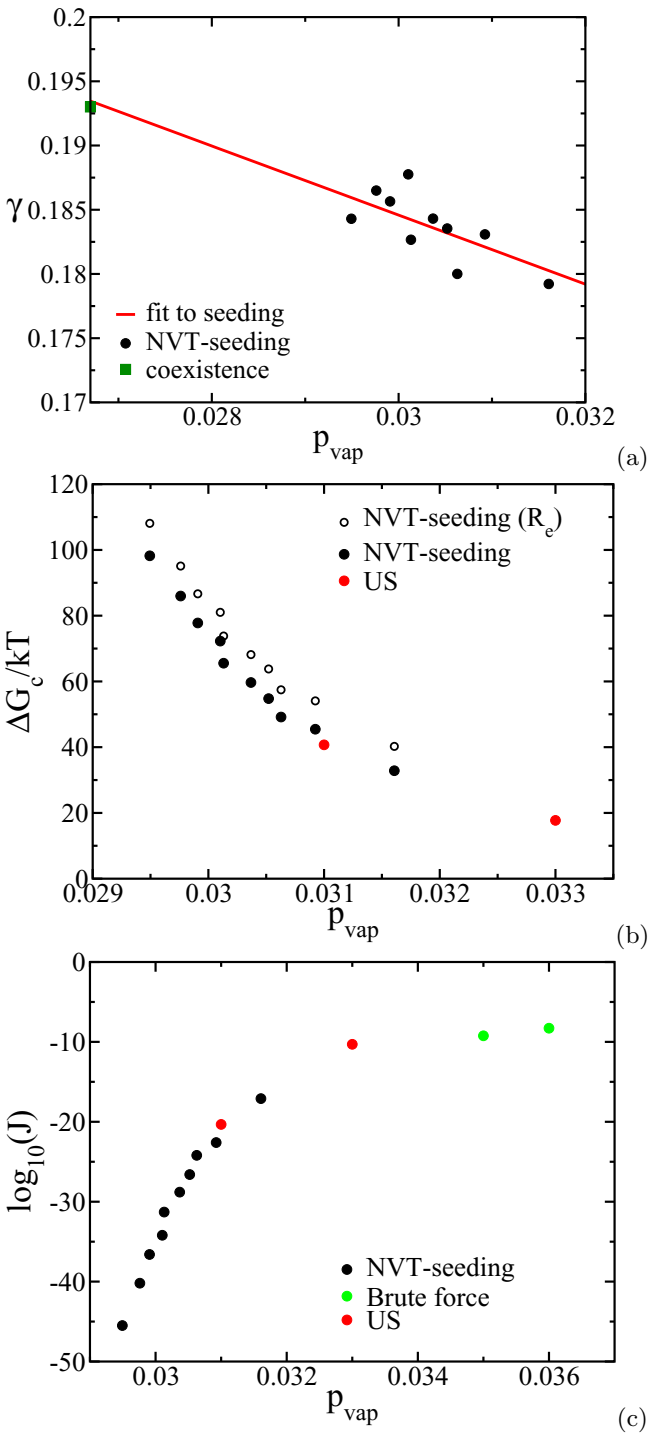

FIG. 4. (a) γ vs vapor pressure obtained from *NVT*-Seeding data of droplets surrounded by supersaturated vapor. The surface tension at coexistence ($p = 0.0267$) is included [70]. (b) ΔG_c vs vapor pressure. *NVT*-Seeding and US data are compared. Empty black symbols correspond to Seeding predictions when the Gibbs dividing (equimolar), instead of the equidensity, surface is employed to identify the cluster radius. (c) Nucleation rate vs vapor pressure as obtained from *NVT*-Seeding, US, and spontaneous nucleation.

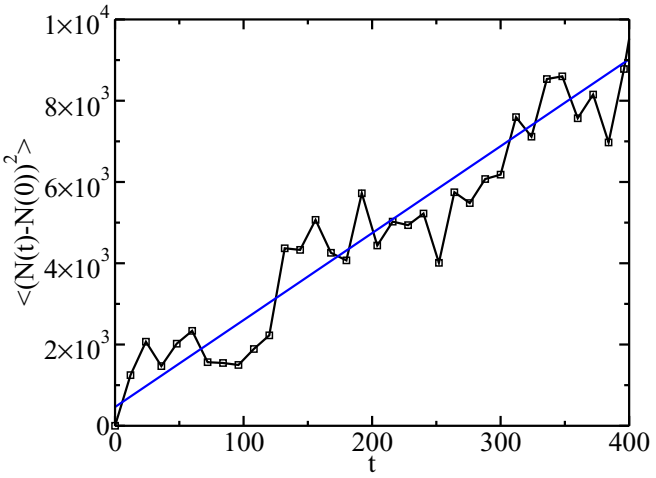

FIG. 5. Time dependence of the mean-squared deviation of the number of particles in the critical drop for system VI in Table I. Half the slope of this plot gives the attachment rate according to Eq. (12).

the critical drop radius with the equidensity distance seems to be quite general for condensation-evaporation transitions.

3. J

Once ΔG_c is known computing J via Eq. (6) is quite straightforward. The kinetic prefactor A_0 given by the kinetic theory of gases, Eq. (10), depends on parameters we already have under control: Δp, R_c, and the density of both phases. The values of A_0 computed via Eq. (10), $A_0^{\rm ktg}$, are reported in Table I.

These A_0 values are approximate since they rely on the validity of the kinetic theory of gases to estimate the attachment rate (see Sec. III). We therefore have to check A_0^{ktg} by computing the attachment rate with an alternative approach. Following the work by Auer and Frenkel [102], the attachment rate can be computed from the diffusion of N, the number of particles in the liquid drop, around the critical drop [102]:

$$f_{\rm af}^{+} = \frac{\langle (N(t) - N(0))^2 \rangle_{Nc}}{2t}, \tag{12}$$

where the average is performed over several trajectories starting from a critical drop configuration. The "af" subscript stresses the fact that this expression of the attachment rate is based on the work by Auer and Frenkel.

To compute N we follow Ref. [103]. We count as neighbors all particles within a 1.625 distance of a tagged particle. Particles with eight or more neighbors are labeled as "liquid." Two liquid particles belong to the same drop if their mutual distance is less than 1.625. An example of the calculation of f^+ according to Eq. (12) is illustrated in Fig. 5. Typically, $\langle N(t) - N(0) \rangle_{N_c}$ is obtained by averaging 20 *NpT* runs started from independent configurations of the critical drop, coming either from *NVT*-Seeding or from US simulations (see Sec. IV). In these runs, the pressure is fixed to the virial value of the simulations were the critical clusters were previously equilibrated. According to Eq. (12), the slope of Fig. 5 divided by 2 gives f^+. Multiplying such f^+ by the Zeldovich factor we get an estimate of the kinetic prefactor, $A_0^{\rm af}$, that does not rely on the kinetic theory of gases. $A_0^{\rm af}$ is reported in Table I for a couple of critical clusters generated with *NVT*-Seeding (systems IV and VI). $A_0^{\rm af}$ is very close to $A_0^{\rm ktg}$. This agreement suggests the validity of the kinetic theory of gases to estimate the attachment rate and makes the theoretical framework that supports the Seeding technique quite powerful given that, since $A_0^{\rm ktg}$ can be used, only R_c, Δp, and the density of both phases are required to get accurate estimates of J in a wide range of orders of magnitude. Note in Fig. 4(c) that Seeding (black dots) has access to J values many orders of magnitude lower than US (red dots).

TABLE II. Data corresponding to the brute force calculations.

Label	N_T	$\langle V \rangle$	p_v	ρ_v	$\log_{10}(J)$
BF-1	4000	57 145	0.035	0.0700	−9.235
BF-2	4000	53 456	0.036	0.0748	−8.287

The green dots in Fig. 4(c) correspond to rate estimates obtained in brute force *NPT* molecular simulation runs performed at high supersaturations where condensation occurs spontaneously from an unseeded vapor. In such cases the nucleation rate can be estimated as $J = 1/(t\langle V \rangle)$, where $\langle V \rangle$ is the average volume before nucleation and t is the nucleation time averaged over a number of independent trajectories (typically 20 in our case). N_T, V, the vapor pressure and density, and J for the two states where we studied spontaneous condensation are reported in Table II. In Fig. 4(c) we show that J estimates from Seeding and from spontaneous nucleation are consistent with each other, which further indicates the ability of Seeding to predict nucleation rates. It is worth mentioning here that *NVT*-Seeding and spontaneous nucleation are complementary techniques. On the one hand, the former does not have access to such high supersaturations given the difficulty to equilibrate small clusters in the *NVT* ensemble [54,55]. That said, it would be nonsense to use Seeding where nucleation occurs spontaneously in a straightforward manner. On the other hand, spontaneous nucleation is limited to a narrow window of nucleation rates (that enabled by computational time), whereas Seeding has access to extremely low rates.

We would like to end this section by discussing finite-size effects, which could be present if a nucleus sees its replica through periodic boundary conditions. On the one hand, we made sure that the density of the outer phase reaches a plateau before $L/2$ by looking at radial density profiles such as that shown in Fig. 2. On the other hand, we note that the box side of system X is more than twice than those of the other systems. By looking at Figs. 4(a), 4(b), and 4(c) one can see that the results from system X are fully consistent with those inferred from the other systems, which strongly supports the absence of noticeable finite-size effects in our simulations.

IV. UMBRELLA SAMPLING

As previously indicated, to validate the Seeding results we used the US technique. We followed Refs. [103,104] to compute ΔG_c for two different vapor pressures: $p = 0.031$ and $p = 0.033$. Details on the simulation box size and number

TABLE III. Data corresponding to the US calculations.

Label	L	N_T	$\Delta G_c/(k_BT)$	$A_0^{\rm af}$	$\log_{10}(J)$
US-1	39.112	4000	17.7	0.041	−10.3
US-2	38.501	4000	40.7	0.039	−20.3

of particles in the systems used to perform the US calculations are given in Table III.

The free energy associated with the formation of an N particle cluster drop can be obtained from

$$\Delta G(N) = -k_BT \ln[P(N)], \tag{13}$$

where $P(N)$ is the probability distribution of N. Our criterion to compute N is described in Sec. III B 3. It is important to note that even though different criteria may give different N for a given configuration, the height of an US free energy barrier does not depend on the criterion to determine the cluster size [73]. Therefore, contrary to what happens in Seeding, the US method does not depend on the specific criterion to determine the nucleus size. This is why it is important to validate the Seeding method with other techniques such us US.

With conventional NpT simulations at the selected pressures $P(N)$ can be sampled only up to $N \sim 40$ while the critical cluster is much larger in this regime. To sample the rest of the free energy barrier a biasing potential, $U_{\rm bias}$, is added to the original Hamiltonian:

$$U_{\rm bias} = \tfrac{1}{2}k_{\rm bias}(N - N_0)^2, \tag{14}$$

where N_0 controls the cluster size around which the sampling will be centered and k the width of such sampling. Tens of overlapping sampling "windows" centered at different N_0 values are required to reconstruct the whole free energy barrier. The effect of the bias potential on the calculation of the free energy barrier is removed as follows [71]:

$$\Delta G(N) = -k_BT \ln\left\langle \frac{\chi_N}{e^{-U_{\rm bias}/(k_BT)}} \right\rangle + C, \tag{15}$$

where χ_N is the fraction of clusters with N particles that appear within a certain window and C is a constant. The constant is obtained by gluing together the first part of the energy barrier evaluated without the biasing potential [Eq. (13)] with the rest of the windows. The result is the whole free energy barrier.

To compute each window we use the hybrid Molecular Dynamics–Monte Carlo scheme labeled as HMC(nM-NpT)/US in Ref. [104]. From the starting configuration, random velocities are assigned to every particle according to a Maxwell-Boltzmann distribution, and a short (Δt 19.2 Lennard-Jones times) MD simulation is run for generating a new configuration, which is accepted with probability $\min[1, \exp\{-[U_{\rm bias}(\Delta t) - U_{\rm bias}(0)]/(k_BT)\}]$. In the case of either acceptance or rejection new random velocities are assigned at the beginning of each short MD cycle. For each window, 10 000 of such cycles were performed for equilibration and 60 000 to obtain the free energy barrier. We used $k_{\rm bias} = 0.04k_BT$ in the biasing potential [Eq. (14)], which gives an acceptance rate of ∼25%.

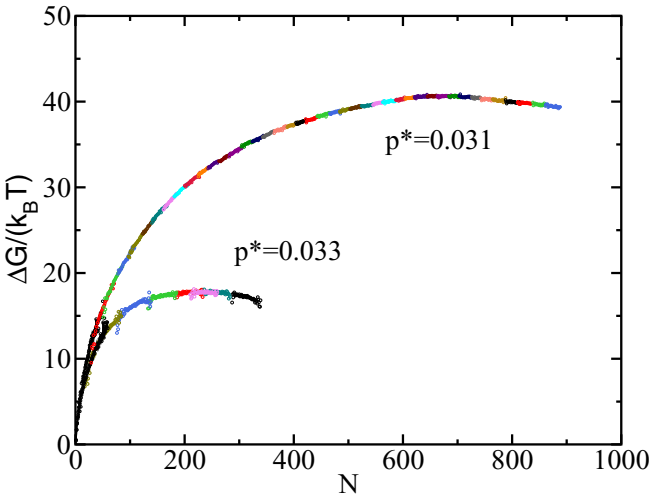

FIG. 6. Free energy for two different pressures ($p = 0.031$ and $p = 0.033$) versus the number of particles in the drop as obtained from US calculations. The different colors represent the different windows performed.

In Fig. 6 we plot both free energy barriers, where $\Delta G_c = 17.7k_BT$ for $p = 0.033$ and $\Delta G_c = 40.7k_BT$ for $p = 0.031$ (also reported in Table III). As already discussed, the agreement between US and Seeding is excellent [see Fig. 4(b)].

Additionally, we compute the kinetic prefactor $A_0^{\rm af}$ [Eq. (7)] to obtain the nucleation rate [Eq. (6)]. To do that, we launch tens of unbiased trajectories from independent configurations at the barrier top in order to compute the attachment rate via Eq. (12). The Zeldovich factor [Eq. (8)] can be obtained by numerically calculating the curvature of $\Delta G(N)$ at the barrier top. We report $A_0^{\rm af}$ thus calculated and the corresponding J in Table III. As previously discussed, J from US is fully consistent with that coming from Seeding [see Fig. 4(c)].

In summary, we have compared Seeding, which relies on the theoretical assumptions by CNT and ktg and depends on the criterion employed to determine the cluster size, with US, which does not have these limitations. We have obtained an excellent agreement between both techniques. This is very good news because Seeding is much more efficient than US and has access to much lower values of the nucleation rate.

V. CONDENSATION VERSUS BOILING

A. Comparison for a given R_c

We have studied quite recently the nucleation of bubbles for the same Lennard-Jones model employed here [54]. Since the study was performed at the same temperature, the question that naturally arises is whether bubbles and drops with the same radius have the same interfacial properties. To establish the comparison we have repeated the analysis performed in Ref. [54] because in that work we used 0.026 as the coexistence pressure instead of 0.0267. We took the 0.026 value from a paper published more than a decade ago [75]. However, we have recomputed more carefully the coexistence pressure at $T = 0.785$ and obtain $p = 0.0267$ instead, which is the value we use in this work. The difference is subtle, but given

TABLE IV. *NVT*-Seeding data for the different bubbles studied in this work at $T = 0.785$.

Label	L	N_T	ρ_{vap}	ρ_l	p_{vap}	p_l	Δp	R_c	γ	$\Delta G_c/(k_BT)$	A_0^{BK}	$\log_{10}(J)$
I	36.731	30795	0.03765	0.6453	0.02365	−0.02601	0.0497	7.35	0.1826	52.7	0.341	−23.5
II	36.731	30342	0.03834	0.6484	0.02398	−0.01914	0.0431	8.50	0.1832	70.6	0.342	−31.3
III	36.731	29760	0.03875	0.6501	0.02419	−0.01503	0.0392	9.53	0.1869	90.6	0.345	−40.0
IV	36.731	29034	0.03907	0.6514	0.02433	−0.01191	0.0362	10.52	0.1906	112.5	0.348	−49.5
V	36.731	28147	0.03949	0.6530	0.02453	−0.00776	0.0323	11.50	0.1857	131.1	0.344	−57.6
VI	36.731	27082	0.03972	0.6539	0.02464	−0.00558	0.0302	12.45	0.1881	155.7	0.346	−68.3

that the pressure inside the nucleating phase is obtained by integrating from the coexistence pressure [see Eq. (11)], it is very important to use an accurate value for the latter.

The simulation data for different bubbles equilibrated at $T = 0.785$ in the *NVT* ensemble are reported in Table IV. The values of R_c corresponding to each system (obtained with the equidensity criterion as discussed in Sec. III A and in Ref. [54]) are very close to those recently reported by ourselves [54]. However, the values of Δp here reported are not identical to those of Ref. [54] due to the coexistence pressure issue discussed above. In Fig. 7(a) we plot Δp versus $1/R_c$ for bubbles and and drops at $T = 0.785$. Drops and bubbles of the same size have the same Δp, which is perhaps the most important result of the paper. Note that, for a given R_c, the pressures of the external and the internal phases are not the same if one compares cavitation and condensation. What is the same is the pressure difference between the internal and the external phases. For instance, let us focus on the case of drop VII and bubble II, both with $R_c \approx 8.5$. In Fig. 8 we compare their radial density profiles. The density of the liquid inside the drop is different from that of the liquid outside the bubble. Also, the density of the vapor inside the bubble is different from that of the vapor outside the drop. The bubble is surrounded by a liquid of pressure −0.01914 whereas the drop by a vapor of pressure 0.0301: the pressures of the external phases do not even have the same sign. The bubble and the drop also have very different pressures: 0.02398 and 0.07432, respectively. Despite the fact that the external and the internal pressures are very different, Δp is not: 0.043 and 0.044 for the bubble and the drop, respectively.

According to the Laplace equation, that $\Delta p(R_c)$ is the same for drops and bubbles, implies that γ also must be the same regardless of the identity of the internal and the external phases. In Fig. 7(b) we plot γ versus $1/R_c$ for bubbles and drops and find that, indeed, they have the same γ within our statistical noise. Of course, attending to Eq. (3), ΔG_c, which depends only on R_c and Δp, is also the same for a given R_c, as illustrated in Fig. 7(c).

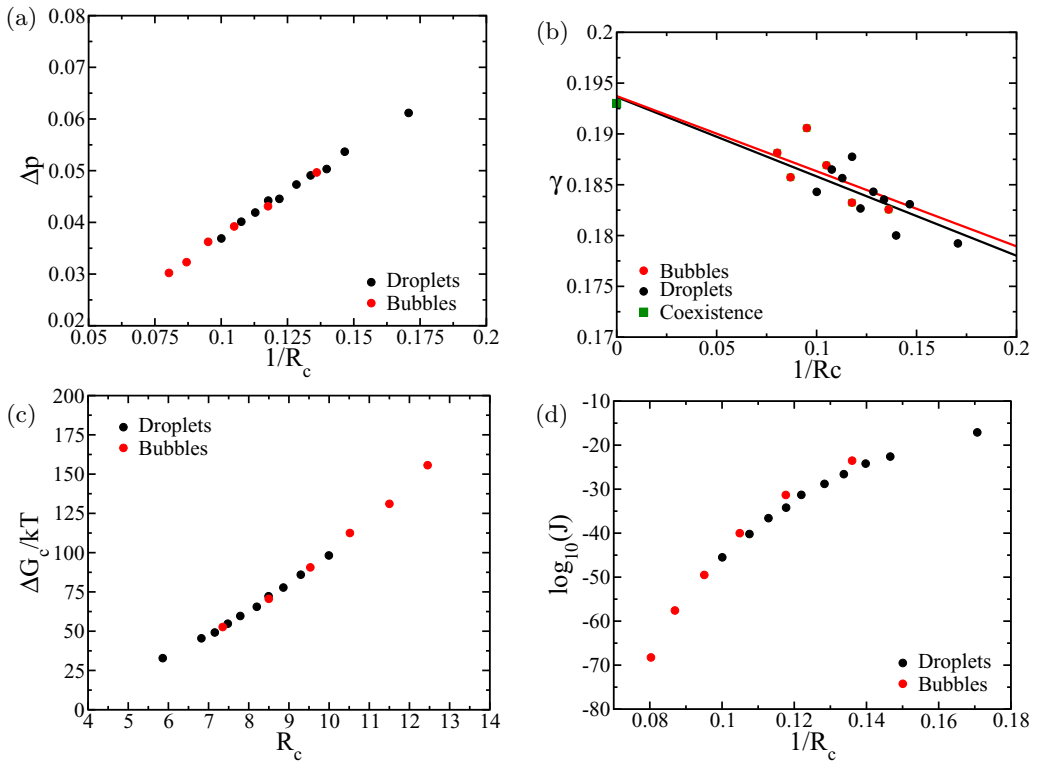

FIG. 7. (a) Δp vs $1/R_c$, (b) γ vs $1/R_c$, (c) ΔG_c vs R_c, and (d) $\log_{10} J$ vs $1/R_c$ for droplets (black symbols) and bubbles (red symbols) as obtained from *NVT*-Seeding.

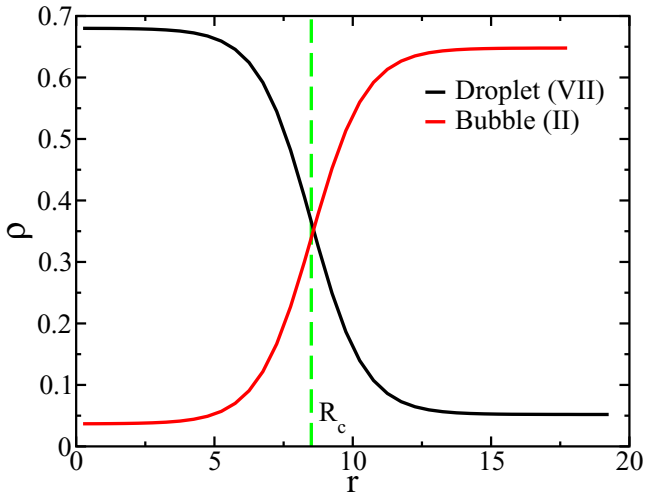

FIG. 8. Radial density profiles of drop VII and bubble II, compared. They have almost identical radius, R_c.

The nucleation rate for bubbles with a given R_c is close to the corresponding drop but is not exactly the same, given that the kinetic prefactor is not identical. In the case of bubble nucleation we have carefully assessed [70] that the following expression by Blander and Katz (BK) provides a good approximation for A_0:

$$A_0^{BK} = \sqrt{\frac{\Delta p R_c}{\pi m}}, \tag{16}$$

which is very similar, but with a missing $(\rho_{\rm vap}/\rho_l)$ factor with respect to the ktg expression we use for drop condensation [Eq. (10)]. The A_0^{BK} values we use in our Seeding predictions of bubble cavitation are reported in Table IV alongside the resulting values of J obtained as $J = \rho_l A_0^{BK} \exp[-\Delta G_c/(k_B T)]$. As can be seen in Fig. 7(d), the rate for bubbles and drops for a given R_c is quite similar, although it is systematically lower for the latter due to the $\rho_{\rm vap}/\rho_l$ factor previously mentioned.

Condensation and cavitation have already been compared in the literature [32,35,43,48,105–107]. However, there are only a few cases in which γ has been compared for a given temperature as a function of the droplet or bubble size [32,35] as we do in this work. Establishing such a comparison in experiments is difficult because it is not possible to detect the critical nucleus. In simulations the nucleus can be visualized, but computing γ is a hard task. It requires either computing the free energy of a system with the nucleus inside [32,34] or, more easily, computing the nucleus size and using a theory to infer γ [60,108] as we do in this work. In either approach, one has to deal with the arbitrariness of establishing a location for the interface.

In our case, we found in a recent work by "trial and error" that the equidensity surface gives good results for cavitation [70]. By "good results" we mean that Seeding predictions of nucleation are consistent with those coming from independent methods that do not rely on a precise definition of the nucleus size. In this work we have demonstrated that the same criterion to locate the interface is successful in condensation. Therefore, one of our main findings is that the equidensity surface is the one that provides good predictions when CNT is used both for cavitation and for condensation. This means that the equidensity surface can be identified with the surface of tension, which is the one for which CNT works and the Laplace equation holds (see Sec. III) [47,49,55,109]. We believe that identifying the surface of tension with the equidensity surface for both cavitation and condensation is an important finding of our work. This leads to the relevant conclusion that condensation and cavitation are two sides of the same coin in the sense that they share the same surface tension.

In Ref. [35] γ was found to be quite different for both phenomena, but the comparison was not established for the surface of tension but for the equimolar surface. In Ref. [32], however, the comparison was established for the surface of tension, and, although γ was similar for condensation and cavitation, there were significant differences that need to be further investigated in order to match our work with that of Ref. [32].

B. Comparison for a given metastability degree

In Ref. [83] it was proposed in a DFT study that the work of formation of critical bubbles studied at different temperatures collapses when plotted against the metastability degree, X_m, quantified as

$$X_m = \frac{\mu_{\rm nuc} - \mu_{\rm coex}}{\mu_{\rm spinodal} - \mu_{\rm coex}}, \tag{17}$$

where $\mu_{\rm nuc}$ is the chemical potential of the parent phase at the conditions where nucleation is studied, $\mu_{\rm coex}$ is the coexistence chemical potential at the same temperature and at coexistence pressure, and $\mu_{\rm spinodal}$ is the chemical potential at the same temperature but at the pressure where spinodal decomposition takes place. To estimate the spinodal pressure we run NpT simulations of the bulk liquid and vapor phases with 4000 particles. We estimate the spinodal decomposition pressure as that for which the system undergoes a phase transition without any induction period, right after the start of the simulation. Both chemical potential differences in Eq. (17) can be easily obtained by numerically integrating the molar volume along pressure at constant temperature. The denominator is the maximum possible metastability, whereas the numerator is the actual metastability of the state where nucleation is studied. Therefore, X_m varies from 0 at coexistence, to 1 at spinodal decomposition. The mestastability degree above described can be computed for drop as well as for bubble nucleation. Therefore, we have the chance to compare nucleation free energy barriers for drops and bubbles as a function of X_m. The comparison, shown in Fig. 9, reveals the interesting conclusion that ΔG_c for bubble and drop nucleation is the same for a given metastbility degree. Therefore, not only can nucleation barriers at different temperatures be collapsed via the metastability degree as proposed in Ref. [83], but bubble and drop nucleation data also match for a given metastability degree.

C. Tolman length

Since bubbles and drops of the same radius have the same interfacial properties, we can use the data coming from both

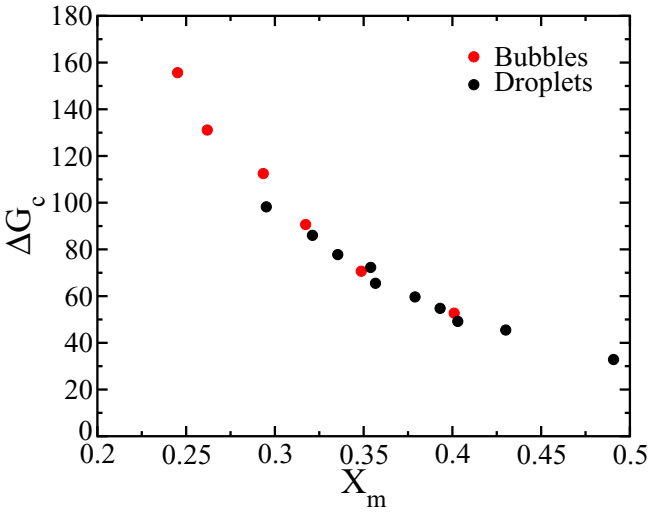

FIG. 9. Nucleation free energy barrier for drops and bubbles (see legend) as a function of the metastability degree, X_m, defined in Eq. (17).

systems altogether in order to compute the Tolmann length, δ_T, which is defined as [34,74]

$$\delta_{\text{Tolman}} = \lim_{R_s \to \infty} (R_e - R_s), \tag{18}$$

where R_e is the Gibbs equimolar radius and R_s is the radius of the surface of tension. We identify R_s with R_c (the equidensity radius) given that (1) we obtain good predictions of nucleation when we use R_c and (2) R_s is the radius that enters CNT [47,49,55,109]. To underline the fact that we identify R_c with R_s we label R_c as $R_{s=c}$ in the following figures. R_e can be easily computed from the radial density profiles [54,55]. In Fig. 10(a) we show $R_e - R_{s=c}$ versus $1/R_{s=c}$ for all data (either bubbles or drops) coming from this work. The extrapolation to $1/R_{s=c} = 0$ provides an estimate of δ_{Tolman}, indicated with an empty blue dot in the figure. We obtain $\delta_{\text{Tolman}} = 0.15 \pm 0.02$. We showed in a recent paper, in which we analyzed spherical hard sphere crystals in equilibrium with the fluid, that δ_{Tolman} can be also estimated by fitting γ to the following expression:

$$\gamma = \gamma_0 \left(1 - 2\frac{\delta_T}{R_s}\right), \tag{19}$$

where γ_0 is the value of γ at coexistence at the temperature of interest and δ_T is the fitting parameter that serves as an estimate for δ_{Tolman} [55]. This approach is similar in spirit to those that include γ given by Eq. (19) in CNT to fit free energy barriers obtained by rare event methods [84,110]. Again, we identify here R_s with R_c. Consequently, we use the γ data coming from such a radius (that reported in Tables I and IV) to obtain an estimate of δ_T with the expression above. The data of γ versus $1/R_{s=c}$ are shown in green in Fig. 10(b). The solid line is a linear fit of γ versus $1/R_{s=c}$, which includes γ_0 (the green square in the figure). The δ_T value coming from such fit, $\delta_T = 0.21 \pm 0.03$, is shown with a red dot in Fig. 10(a). Both values, δ_{Tolman} obtained via Eq. (18) [blue dot in Fig. 10(a)] and δ_T coming from Eq. (19) (red dot in the same figure), are consistent with each other within the statistical uncertainty of our estimates. This corroborates the idea, recently checked

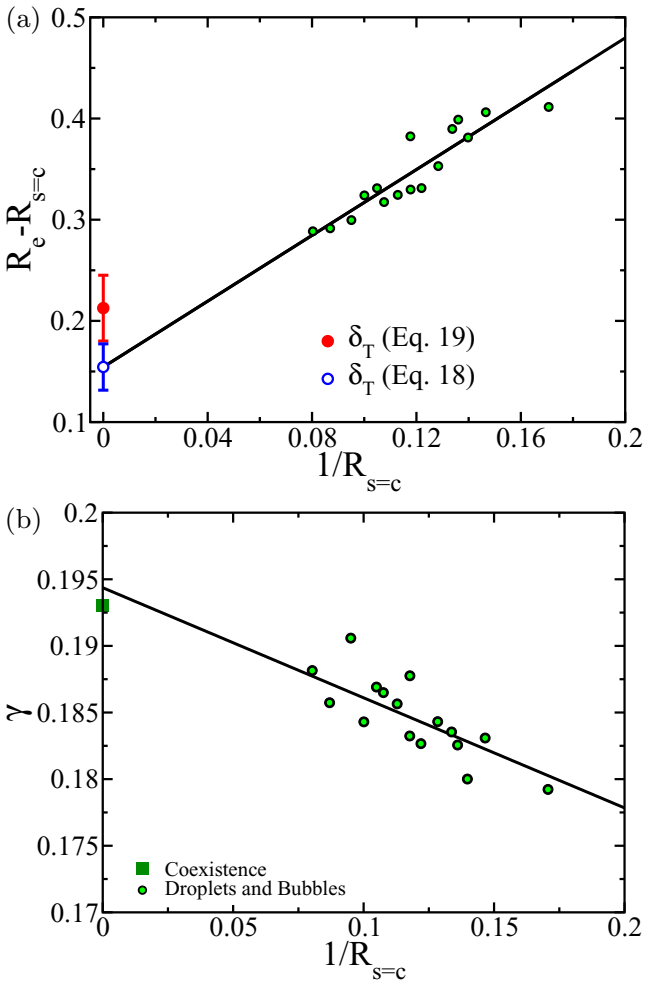

FIG. 10. (a) $R_e - R_{s=c}$ and (b) γ vs $1/R_{s=c}$ for drops and bubbles together.

for hard sphere crystals [55], that the Tolman length can be obtained either from Eq. (19) or from Eq. (18). Hence, this idea seems to be a general one pertaining not only to the crystal-fluid equilibrium but also to the liquid-vapor one.

This study may shed some light in the intense literature debate about the magnitude and sign of the Tolman length [18,30–32,34–44]. We obtain a Tolman length of about 20% of the particle diameter. Its sign is positive, which means that γ decreases when one moves away from coexistence at constant temperature.

VI. CONCLUSIONS

The main conclusions we draw from our work are the following:

(1) We have used *NVT*-Seeding to investigate droplet nucleation in a supersaturated Lennard-Jones vapor. The results obtained from this technique are consistent with the following: (i) independent calculations of the nucleation free energy barrier performed with Umbrella Sampling, (ii) the surface tension of a flat interface obtained from the pressure tensor in a vapor-liquid coexistence simulation, and (iii) the drop

nucleation rate obtained both with US and in brute force spontaneous nucleation simulations.

(2) *NVT*-Seeding requires defining the radius of a droplet equilibrated in the *NVT* ensemble. The radius definition that passes the consistency tests mentioned in point (1) is that given by the surface where the density is average between that of the interior and that of the exterior phases. Such a radius definition was also successful in our earlier studies of bubble nucleation [54,70]. Therefore, we identify this "equidensity" radius with the radius of tension, R_s.

(3) The good performance of Seeding strongly supports the use of CNT to describe nucleation. However, the capillarity approximation (that γ is curvature independent) does not provide good results. A γ dependent on the curvature of the critical nucleus must be plugged into the the theory. Therefore, the theory, although powerful, requires the involvement of simulations given that the γ-curvature dependence is obtained by computing the size of the critical cluster at different pressures.

(4) The kinetic theory of gases provides very good estimates of the kinetic prefactor of the condensation nucleation rate. This makes the theoretical framework very powerful given that only the size of the critical cluster, the density of the external phase, and the bulk phases equations of state are needed to estimate nucleation rates.

(5) We compare *NVT*-Seeding results of droplets with those obtained for bubbles and find that, for a given temperature, bubbles and droplets of the same radius have, within the accuracy of our method, the same pressure difference with the surrounding medium. Therefore, bubbles and droplets of the same size have the same surface tension and the same nucleation free energy barrier. In this respect, condensation and boiling can be seen as two sides of the same coin. Such duality is verified only if the size of the critical nucleus (either a bubble or a drop) is determined with the equidensity radius (our empirical definition of the surface of tension).

(6) We estimate the Tolman length, δ_T, by extrapolating to infinite-size drops and bubbles the difference between the equimolar radius, R_e, and R_s. Such δ_T is consistent with that obtained by linearly fitting $\gamma(1/R_c)$, in accordance with our recent work on hard sphere crystals [55].

ACKNOWLEDGMENTS

This work was funded by Grants No. FIS2016/78117-P and No. PID2019-105898GB-C21 of the MEC. The authors acknowledge the computer resources and technical assistance provided by the RES. P.R. acknowledges a doctoral grant from UCM. P.M.H. acknowledges financial support from the FPI Grant No. BES- 671 2017-080074. We also thank the reviewers of this work for their suggestions.

[1] G. J. Morris and E. Acton, Controlled ice nucleation in cryopreservation—A review, Cryobiology **66**, 85 (2013).
[2] W. Cantrell and A. Heymsfield, Production of ice in tropospheric clouds: A review, Bull. Am. Meteorol. Soc. **86**, 795 (2005).
[3] P. G. Debenedetti, *Metastable Liquids: Concepts and Principles* (Princeton University Press, Princeton, 1996).
[4] K. T. Smith, Water ice cliffs on mars, Science **359**, 172 (2018).
[5] R. W. Hartel, *Crystallization in Foods* (Springer, New York, 2001).
[6] H. G. Brittain (editor), *Polymorphism in Pharmaceutical Solids* (Marcel Dekker, New York, 1999).
[7] K. F. Kelton, *Crystal Nucleation in Liquids and Glasses* (Academic Press, Boston, 1991).
[8] V. P. Skripov, *Metastable Liquids* (Wiley, New York, 1974).
[9] B. E. Wyslouzil and J. Wölk, Overview: Homogeneous nucleation from the vapor phase: The experimental science, J. Chem. Phys. **145**, 211702 (2016).
[10] P. V. Skripov and A. P. Skripov, The phenomenon of superheat of liquids: In memory of Vladimir P. Skripov, Int. J. Thermophys. **31**, 816 (2010).
[11] E. Lipnyagov, A. Gurashkin, A. Starostin, and P. Skripov, Going to spontaneous boiling-up onset, J. Eng. Thermophys. **27**, 307 (2018).
[12] V. Skripov, Metastable states, J. Non-Equilib. Thermodyn. **17**, 193 (1992).
[13] A. Manka, H. Pathak, S. Tanimura, J. Wolk, R. Strey, and B. E. Wyslouzil, Freezing water in no man's land, Phys. Chem. Chem. Phys. **14**, 4505 (2012).
[14] A. J. Amaya and B. E. Wyslouzil, Ice nucleation rates near ∼225 K, J. Chem. Phys. **148**, 084501 (2018).
[15] X. L. Hu and A. Michaelides, Water on the hydroxylated (0 0 1) surface of kaolinite: From monomer adsorption to a flat 2D wetting layer, Surf. Sci. **602**, 960 (2008).
[16] A. Bhabhe, H. Pathak, and B. E. Wyslouzil, Freezing of heavy water (D_2O) nanodroplets, J. Phys. Chem. A **117**, 5472 (2013).
[17] L. Ickes, A. Welti, C. Hoose, and U. Lohmann, Classical nucleation theory of homogeneous freezing of water: Thermodynamic and kinetic parameters, Phys. Chem. Chem. Phys. **17**, 5514 (2015).
[18] N. Bruot and F. Caupin, Curvature dependence of the liquid-vapor surface tension beyond the Tolman approximation, Phys. Rev. Lett. **116**, 056102 (2016).
[19] L. Granasy, T. Pusztai, and P. F. James, Interfacial properties deduced from nucleation experiments: A Cahn–Hilliard analysis, J. Chem. Phys. **117**, 6157 (2002).
[20] J. G. Kirkwood and F. P. Buff, The statistical mechanical theory of surface tension, J. Chem. Phys. **17**, 338 (1949).
[21] G. Gloor, G. Jackson, F. Blas, and E. de Miguel, Test-area simulation method for the direct determination of the interfacial tension of systems with continuous or discontinuous potentials, J. Chem. Phys. **123**, 134703 (2005).
[22] J. Q. Broughton and G. H. Gilmer, Molecular dynamics investigation of the crystal–fluid interface. VI. Excess surface free energies of crystal–liquid systems, J. Chem. Phys. **84**, 5759 (1986).
[23] J. J. Hoyt, M. Asta, and A. Karma, Method for Computing the Anisotropy of the Solid-Liquid Interfacial Free Energy, Phys. Rev. Lett. **86**, 5530 (2001).
[24] A. Laio and M. Parrinello, Escaping free-energy minima, Proc. Natl. Acad. Sci. USA **99**, 12562 (2002).

[25] S. Angioletti-Uberti, M. Ceriotti, P. D. Lee, and M. W. Finnis, Solid-liquid interface free energy through metadynamics simulations, Phys. Rev. B **81**, 125416 (2010).
[26] L. A. Fernandez, V. Martin-Mayor, B. Seoane, and P. Verrocchio, Equilibrium Fluid-Solid Coexistence of Hard Spheres, Phys. Rev. Lett. **108**, 165701 (2012).
[27] T. Zykova-Timan, D. Ceresoli, U. Tartaglino, and E. Tosatti, Why are Alkali Halide Surfaces not Wetted by Their Own Melt? Phys. Rev. Lett. **94**, 176105 (2005).
[28] S. Auer and D. Frenkel, Prediction of absolute crystal-nucleation rate in hard-sphere colloids, Nature (London) **409**, 1020 (2001).
[29] J. R. Espinosa, C. Vega, and E. Sanz, The mold integration method for the calculation of the crystal-fluid interfacial free energy from simulations, J. Chem. Phys. **141**, 134709 (2014).
[30] G. V. Lau, I. J. Ford, P. A. Hunt, E. A. Müller, and G. Jackson, Surface thermodynamics of planar, cylindrical, and spherical vapour-liquid interfaces of water, J. Chem. Phys. **142**, 114701 (2015).
[31] B. Cheng and M. Ceriotti, Communication: Computing the Tolman length for solid-liquid interfaces, J. Chem. Phys. **148**, 231102 (2018).
[32] K. Binder, B. J. Block, P. Virnau, and A. Tröster, Beyond the van der Waals loop: What can be learned from simulating Lennard-Jones fluids inside the region of phase coexistence, Am. J. Phys. **80**, 1099 (2012).
[33] J. S. Rowlinson and B. Widom, *Molecular Theory of Capillarity* (Courier Corporation, Indianapolis, 2013).
[34] E. M. Blokhuis and J. Kuipers, Thermodynamic expressions for the Tolman length, J. Chem. Phys. **124**, 074701 (2006).
[35] B. J. Block, S. K. Das, M. Oettel, P. Virnau, and K. Binder, Curvature dependence of surface free energy of liquid drops and bubbles: A simulation study, J. Chem. Phys. **133**, 154702 (2010).
[36] J. G. Sampayo, A. Malijevský, E. A. Müller, E. de Miguel, and G. Jackson, Communications: Evidence for the role of fluctuations in the thermodynamics of nanoscale drops and the implications in computations of the surface tension, J. Chem. Phys. **132**, 141101 (2010).
[37] A. Malijevský and G. Jackson, A perspective on the interfacial properties of nanoscopic liquid drops, J. Phys.: Condens. Matter **24**, 464121 (2012).
[38] H. M. Lu and Q. Jiang, Size-dependent surface tension and Tolman's length of droplets, Langmuir **21**, 779 (2005).
[39] S. M. Thompson, K. E. Gubbins, J. P. R. B. Walton, R. A. R. Chantry, and J. S. Rowlinson, A molecular dynamics study of liquid drops, J. Chem. Phys. **81**, 530 (1984).
[40] J. Vrabec, G. K. Kedia, G. Fuchs, and H. Hasse, Comprehensive study of the vapour–liquid coexistence of the truncated and shifted Lennard–Jones fluid including planar and spherical interface properties, Mol. Phys. **104**, 1509 (2006).
[41] Ø. Wilhelmsen, D. Bedeaux, and D. Reguera, Tolman length and rigidity constants of the Lennard-Jones fluid, J. Chem. Phys. **142**, 064706 (2015).
[42] M. N. Joswiak, R. Do, M. F. Doherty, and B. Peters, Energetic and entropic components of the Tolman length for mW and TIP4P/2005 water nanodroplets, J. Chem. Phys. **145**, 204703 (2016).
[43] J. W. Schmelzer, A. S. Abyzov, and V. G. Baidakov, Entropy and the Tolman parameter in nucleation theory, Entropy **21**, 670 (2019).
[44] D. Richard and T. Speck, Crystallization of hard spheres revisited. II. Thermodynamic modeling, nucleation work, and the surface of tension, J. Chem. Phys. **148**, 224102 (2018).
[45] M. Schrader, P. Virnau, and K. Binder, Simulation of vapor-liquid coexistence in finite volumes: A method to compute the surface free energy of droplets, Phys. Rev. E **79**, 061104 (2009).
[46] M. Matsumoto and K. Tanaka, Nano bubble-size dependence of surface tension and inside pressure, Fluid Dyn. Res. **40**, 546 (2008).
[47] A. Tröster, M. Oettel, B. Block, P. Virnau, and K. Binder, Numerical approaches to determine the interface tension of curved interfaces from free energy calculations, J. Chem. Phys. **136**, 064709 (2012).
[48] L. G. MacDowell, V. K. Shen, and J. R. Errington, Nucleation and cavitation of spherical, cylindrical, and slablike droplets and bubbles in small systems, J. Chem. Phys. **125**, 034705 (2006).
[49] A. Statt, P. Virnau, and K. Binder, Finite-Size Effects on Liquid-Solid Phase Coexistence and the Estimation of Crystal Nucleation Barriers, Phys. Rev. Lett. **114**, 026101 (2015).
[50] P. Koß, A. Statt, P. Virnau, and K. Binder, The phase coexistence method to obtain surface free energies and nucleation barriers: A brief review, Mol. Phys. **116**, 2977 (2018).
[51] K. Gunawardana and X. Song, Theoretical prediction of crystallization kinetics of a supercooled Lennard-Jones fluid, J. Chem. Phys. **148**, 204506 (2018).
[52] J. Zierenberg and W. Janke, Exploring different regimes in finite-size scaling of the droplet condensation-evaporation transition, Phys. Rev. E **92**, 012134 (2015).
[53] J. Zierenberg, P. Schierz, and W. Janke, Canonical free-energy barrier of particle and polymer cluster formation, Nat. Commun. **8**, 14546 (2017).
[54] P. Rosales-Pelaez, I. Sanchez-Burgos, C. Valeriani, C. Vega, and E. Sanz, Seeding approach to nucleation in the *NVT* ensemble: The case of bubble cavitation in overstretched Lennard Jones fluids, Phys. Rev. E **101**, 022611 (2020).
[55] P. Montero de Hijes, J. R. Espinosa, V. Bianco, E. Sanz, and C. Vega, Interfacial free energy and Tolman length of curved liquid–solid interfaces from equilibrium studies, J. Phys. Chem. C **124**, 8795 (2020).
[56] J. F. Lutsko and J. Lam, Classical density functional theory, unconstrained crystallization, and polymorphic behavior, Phys. Rev. E **98**, 012604 (2018).
[57] J. F. Lutsko, How crystals form: A theory of nucleation pathways, Science Adv. **5**, eaav7399 (2019).
[58] E. Sanz, C. Vega, J. R. Espinosa, R. Caballero-Bernal, J. L. F. Abascal, and C. Valeriani, Homogeneous ice nucleation at moderate supercooling from molecular simulation, J. Am. Chem. Soc. **135**, 15008 (2013).
[59] B. C. Knott, V. Molinero, M. F. Doherty, and B. Peters, Homogeneous nucleation of methane hydrates: Unrealistic under realistic conditions, J. Am. Chem. Soc. **134**, 19544 (2012).
[60] X.-M. Bai and M. Li, Calculation of solid-liquid interfacial free energy: A classical nucleation theory based approach, J. Chem. Phys. **124**, 124707 (2006).

[61] J. R. Espinosa, C. Vega, C. Valeriani, and E. Sanz, Seeding approach to crystal nucleation, J. Chem. Phys. **144**, 034501 (2016).
[62] M. Volmer and A. Weber, Keimbildung in übersattigten Gebilden, Z. Phys. Chem. **119**, 277 (1926).
[63] R. Becker and W. Doring, Kinetische Behandlung der Keimbildung in übersattigten Dampfen, Ann. Phys. **416**, 719 (1935).
[64] J. W. Gibbs, On the equilibrium of heterogeneous substances, Trans. Connect. Acad. Sci. **3**, 108 (1876).
[65] J. W. Gibbs, On the equilibrium of heterogeneous substances, Trans. Connect. Acad. Sci. **16**, 343 (1878).
[66] A. Zaragoza, M. M. Conde, J. R. Espinosa, C. Valeriani, C. Vega, and E. Sanz, Competition between ices Ih and Ic in homogeneous water freezing, J. Chem. Phys. **143**, 134504 (2015).
[67] J. R. Espinosa, A. Zaragoza, P. Rosales-Pelaez, C. Navarro, C. Valeriani, C. Vega, and E. Sanz, Interfacial Free Energy as the Key to the Pressure-Induced Deceleration of Ice Nucleation, Phys. Rev. Lett. **117**, 135702 (2016).
[68] J. R. Espinosa, G. D. Soria, J. Ramirez, C. Valeriani, C. Vega, and E. Sanz, Role of salt, pressure, and water activity on homogeneous ice nucleation, J. Phys. Chem. Lett. **8**, 4486 (2017).
[69] J. R. Espinosa, C. Vega, and E. Sanz, Homogeneous ice nucleation rate in water droplets, J. Phys. Chem. C **122**, 22892 (2018).
[70] P. Rosales-Pelaez, M. I. Garcia-Cid, C. Valeriani, C. Vega, and E. Sanz, Seeding approach to bubble nucleation in superheated Lennard-Jones fluids, Phys. Rev. E **100**, 052609 (2019).
[71] G. M. Torrie and J. P. Valleau, Monte carlo free energy estimates using non-Boltzmann sampling: Application to the sub-critical Lennard-Jones fluid, Chem. Phys. Lett. **28**, 578 (1974).
[72] J. S. van Duijneveld and D. Frenkel, Computer simulation study of free energy barriers in crystal nucleation, J. Chem. Phys. **96**, 4655 (1992).
[73] L. Filion, M. Hermes, R. Ni, and M. Dijkstra, Crystal nucleation of hard spheres using molecular dynamics, umbrella sampling, and forward flux sampling: A comparison of simulation techniques, J. Chem. Phys. **133**, 244115 (2010).
[74] R. C. Tolman, The effect of droplet size on surface tension, J. Chem. Phys. **17**, 333 (1949).
[75] Z.-J. Wang, C. Valeriani, and D. Frenkel, Homogeneous bubble nucleation driven by local hot spots: A molecular dynamics study, J. Phys. Chem. B **113**, 3776 (2008).
[76] K. K. Tanaka, H. Tanaka, R. Angelil, and J. Diemand, Simple improvements to classical bubble nucleation models, Phys. Rev. E **92**, 022401 (2015).
[77] S. L. Meadley and F. A. Escobedo, Thermodynamics and kinetics of bubble nucleation: Simulation methodology, J. Chem. Phys. **137**, 074109 (2012).
[78] S. Plimpton, Fast parallel algorithms for short-range molecular dynamics, J. Comput. Phys. **117**, 1 (1995).
[79] R. W. Hockney, S. P. Goel, and J. Eastwood, Quiet high resolution computer models of a plasma, J. Comp. Phys. **14**, 148 (1974).
[80] S. Nosé, A unified formulation of the constant temperature molecular dynamics methods, J. Chem. Phys. **81**, 511 (1984).
[81] V. Baidakov and K. Protsenko, Molecular dynamics simulation of cavitation in a Lennard-Jones liquid at negative pressures, Chem. Phys. Lett. **760**, 138030, (2020).
[82] C Valeriani, E Sanz, and D Frenkel, Rate of homogeneous crystal nucleation in molten NaCl, J. Chem. Phys. **122**, 194501 (2005).
[83] V. K. Shen and P. G. Debenedetti, Density-functional study of homogeneous bubble nucleation in the stretched Lennard-Jones fluid, J. Chem. Phys. **114**, 4149 (2001).
[84] M. Gallo, F. Magaletti, D. Cocco, and C. M. Casciola, Nucleation and growth dynamics of vapour bubbles, J. Fluid Mech. **883**, A14 (2020).
[85] J. F. Lutsko, Density functional theory of inhomogeneous liquids. III. Liquid-vapor nucleation, J. Chem. Phys. **129**, 244501 (2008).
[86] D. Kashchiev, On the relation between nucleation work, nucleus size, and nucleation rate, J. Chem. Phys. **76**, 5098 (1982).
[87] D. Kashchiev, Forms and applications of the nucleation theorem, J. Chem. Phys. **125**, 014502 (2006).
[88] J. Wedekind and D. Reguera, What is the best definition of a liquid cluster at the molecular scale? J. Chem. Phys. **127**, 154516 (2007).
[89] S. Marchio, S. Meloni, A. Giacomello, C. Valeriani, and C. Casciola, Pressure control in interfacial systems: Atomistic simulations of vapor nucleation, J. Chem. Phys. **148**, 064706 (2018).
[90] P. Montero de Hijes, K. Shi, E. G. Noya, E. E. Santiso, K. E. Gubbins, E. Sanz, and C. Vega, The Young-Laplace equation for a solid-liquid interface, J. Chem. Phys. **153**, 191102, (2020).
[91] O. Vincent and P. Marmottant, On the statics and dynamics of fully confined bubbles, J. Fluid Mech. **827**, 194 (2017).
[92] D. Marti, Y. Krüger, D. Fleitmann, M. Frenz, and J. Rička, The effect of surface tension on liquid–gas equilibria in isochoric systems and its application to fluid inclusions, Fluid Phase Equilib. **314**, 13 (2012).
[93] J. Wedekind, D. Reguera, and R. Strey, Finite-size effects in simulations of nucleation, J. Chem. Phys. **125**, 214505 (2006).
[94] D. Reguera and H. Reiss, Fusion of the Extended Modified Liquid Drop Model for Nucleation and Dynamical Nucleation Theory, Phys. Rev. Lett. **93**, 165701 (2004).
[95] D. Reguera, R. K. Bowles, Y. Djikaev, and H. Reiss, Phase transitions in systems small enough to be clusters, J. Chem. Phys. **118**, 340 (2003).
[96] P. Koß, A. Statt, P. Virnau, and K. Binder, Free energy barriers for crystal nucleation from fluid phases, Phys. Rev. E **96**, 042609 (2020).
[97] A. J.-M. Yang, The thermodynamical stability of the heterogeneous system with a spherical interface, J. Chem. Phys. **82**, 2082 (1985).
[98] M. Gallo, F. Magaletti, and C. M. Casciola, Thermally activated vapor bubble nucleation: The Landau-Lifshitz–van der Waals approach, Phys. Rev. Fluids **3**, 053604 (2018).
[99] M. Gallo, F. Magaletti, and C. M. Casciola, Heterogeneous bubble nucleation dynamics, J. Fluid Mech. **906**, A20 (2020).
[100] Q. Xiao, Y. Liu, Z. Guo, Z. Liu, D. Frenkel, J. Dobnikar, and X. Zhang, What experiments on pinned nanobubbles can tell about the critical nucleus for bubble nucleation, Eur. Phys. J. E **40**, 114 (2017).

[101] J. Walton, D. Tildesley, J. Rowlinson, and J. Henderson, The pressure tensor at the planar surface of a liquid, Mol. Phys. **48**, 1357 (1983).

[102] S. Auer and D. Frenkel, Numerical prediction of absolute crystallization rates in hard-sphere colloids, J. Phys.: Condens. Matter **120**, 3015 (2004).

[103] P. R. ten Wolde and D. Frenkel, Computer simulation study of gas-liquid nucleation in a Lennard-Jones system, J. Chem. Phys. **109**, 9901 (1998).

[104] M. A. Gonzalez, E. Sanz, C. McBride, J. L. F. Abascal, C. Vega, and C. Valeriani, Nucleation free-energy barriers with hybrid Monte-Carlo/umbrella sampling, Phys. Chem. Chem. Phys. **16**, 24913 (2014).

[105] R. Guermeur, F. Biquard, and C. Jacolin, Density profiles and surface tension of spherical interfaces. numerical results for nitrogen drops and bubbles, J. Chem. Phys. **82**, 2040 (1985).

[106] L. G. MacDowell, P. Virnau, M. Müller, and K. Binder, The evaporation/condensation transition of liquid droplets, J. Chem. Phys. **120**, 5293 (2004).

[107] F. Caupin, Escaping the no man's land: Recent experiments on metastable liquid water, J. Non-Cryst. Solids **407**, 441 (2015).

[108] R. G. Pereyra, I. Szleifer, and M. A. Carignano, Temperature dependence of ice critical nucleus size, J. Chem. Phys. **135**, 034508 (2011).

[109] D. Kashchiev, *Nucleation: Basic Theory with Applications* (Butterworth-Heinemann, Oxford, 2000).

[110] G. Menzl, M. A. Gonzalez, P. Geiger, F. Caupin, J. L. Abascal, C. Valeriani, and C. Dellago, Molecular mechanism for cavitation in water under tension, Proc. Natl. Acad. Sci. USA **113**, 13582 (2016).